Chemical Science

Antiparallel three-component gradients in double-channel surface architectures

Journal:	*Chemical Science*
Manuscript ID:	SC-EDG-07-2014-002092.R1
Article Type:	Edge Article
Date Submitted by the Author:	25-Aug-2014
Complete List of Authors:	Hayashi, Hironobu; Nara Institute of Science and Technology, Sobczuk, Adam; University of Geneva, Department of Organic Chemistry Bolag, Altan; University of Geneva, Department of Organic Chemistry Sakai, Naomi; University of Geneva, Department of Organic Chemistry Matile, Stefan; University of Geneva, Department of Organic Chemistry

Cite this: DOI: 10.1039/c0xx00000x

www.rsc.org/xxxxxx

ARTICLE TYPE

Antiparallel three-component gradients in double-channel surface architectures†

Hironobu Hayashi,[a,b] Adam Sobczuk,[a] Altan Bolag,[a] Naomi Sakai[a] and Stefan Matile*[a]

Received (in XXX, XXX) Xth XXXXXXXXX 200X, Accepted Xth XXXXXXXXX 200X

DOI: 10.1039/b000000x

The synthesis of multicomponent surface architectures of a so far inaccessible level of sophistication is accomplished, and the functional relevance of this unprecedented structural complexity is demonstrated. Co-axial channels of oligothiophenes and fullerenes for the transport of holes and electrons, respectively, are equipped with oriented antiparallel redox gradients with up to three components each to drive the charges apart after their generation with light. In the resulting photosystems, charge recombination decreases with each level of sophistication from 29% to 2%, approaching complete suppression. Photocurrents increase correspondingly, and thermal activation barriers decrease. Increasing turn-on voltages for dark currents indicate that charges struggle to move backward up the gradients with increasing number of components. These results demonstrate that the transcription of most complex lesson from nature to organic materials is possible and worthwhile and thus support curiosity-driven efforts to learn how to synthesize multicomponent architectures of highest possible sophistication with highest possible precision.

Significant biological function is often accomplished by supramolecular architectures of overwhelming complexity.[1] No one knows what we would get from organic materials of comparable sophistication because the methods for their synthesis remain rudimentary despite significant efforts worldwide.[1-17] Particularly challenging is synthetic control over the directionality of multicomponent architectures. However, this directionality is of scientific interest for many reasons. In biological photosystems, for example, electrons and holes, after their generation with light, are guided in opposite directions along oriented multicomponent redox gradients in separate charge-transporting pathways.[1] Whereas molecular systems with co-axial hole (h^+) and electron (e^-) transporting channels have been synthesized,[1-21] the installation of oriented antiparallel multicomponent gradients in these co-axial channels remains difficult because it requires directionality.[1] To contribute to synthetic methods that control directionality in multicomponent architectures, we have introduced zipper assembly[22] and self-organizing surface-initiated polymerization (SOSIP).[23] Robust and user-friendly, SOSIP has been further expanded to include templated self-sorting (TSS)[24] and templated stack exchange (TSE).[25] Here, we use SOSIP-TSE to synthesize the first double-channel architecture with oriented antiparallel redox gradients composed of three components each, and show that this [3+3] architecture, as sophisticated as it gets today, is functionally relevant.

The complete series of [1+1] photosystem **1** with co-axial channels but without gradients, [2+2] photosystem **2** with antiparallel gradients composed of two components each, and the ultimate "triple-gradient" [3+3] photosystem **3** was designed as follows (Fig. 1). Oligothiophenes[26] and fullerenes[27] were selected as hole and electron transporters, respectively. For gradients in the *p*-channel, we envisioned to raise and lower the HOMO energy of quaterthiophenes (TT)[13,26] with two ethylenedioxythiophenes (TE)[13,28,29] and two thiazoles (TA)[13,30,31] in the middle of the tetramer, respectively. In the *n*-channel, the LUMO level of Bingel fullerenes (SB) has been shown to gradually rise in double-bingel fullerenes (DB) and double-bingel methanofullerenes (DM).[7,15,16,27] Architectures needed for control experiments included the gradient-free single-channel [1+0] photosystem **4**.

The components **5-11** were further equipped with all that is needed for SOSIP-TSE (Figs. 1, 2, S1†).[25] To both termini of the TA oligomer in **5** were added i) two diphosphonate "feet" to bind to the indium tin oxide (ITO) surface, ii) a naphthalenediimide (NDI) to template for TSE and iii) a protected cysteine to initiate disulfide-exchange polymerization (Fig. 2A). The termini of TA, TT and TE oligomers in **6-8** all contain i) a benzaldehyde-protected hydrazide for TSE and ii) a strained cyclic disulfide from asparagusic acid to propagate the ring-opening

[a] *Department of Organic Chemistry, University of Geneva, Geneva, Switzerland. Fax: +41 22 379 5123; Tel: +41 22 379 6523; E-mail: stefan.matile@unige.ch; www.unige.ch/sciences/chiorg/matile/*

[b] *Present address: Graduate School of Materials Science, Nara Institute of Science and Technology (NAIST), Nara, Japan.*

†Electronic Supplementary Information (ESI) available: Detailed procedures and results for all reported experiments. See DOI: 10.1039/b000000x/

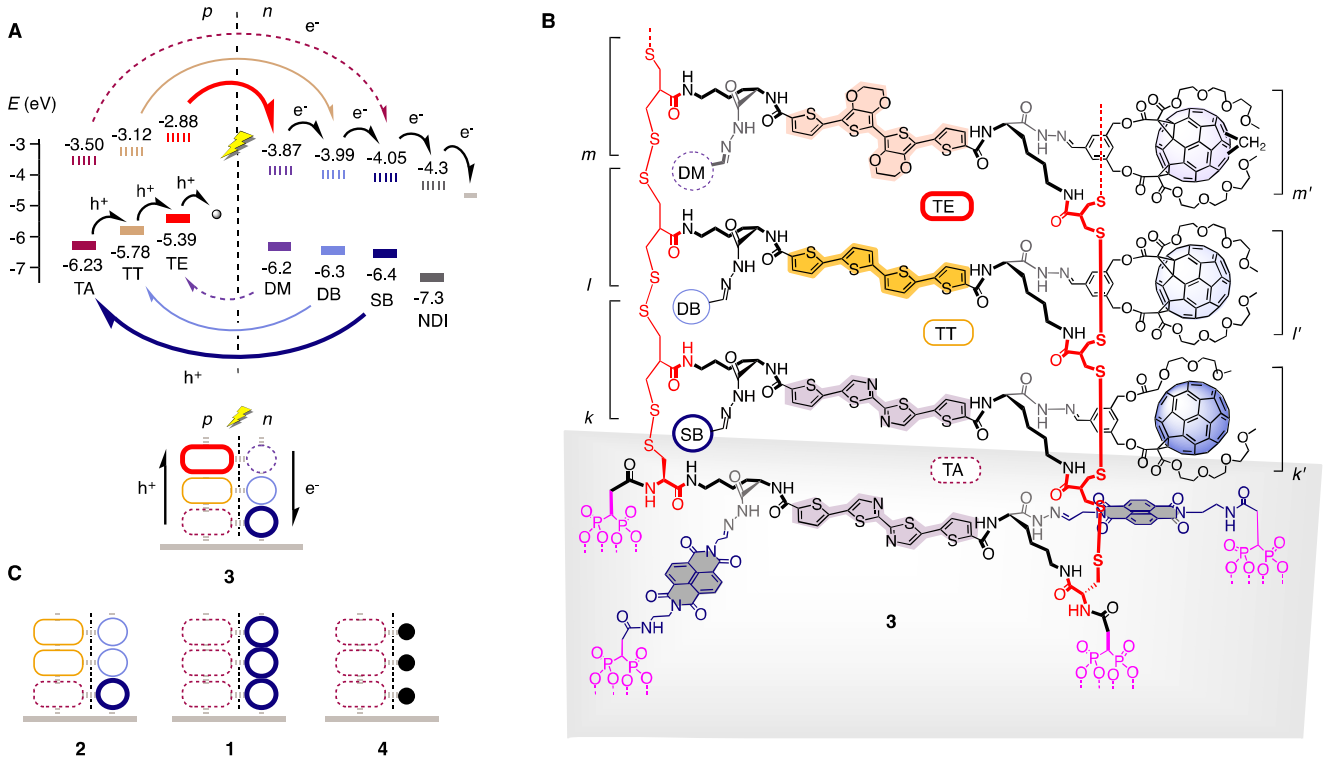

Fig. 1. Design of antiparallel three-component gradients. (A) Schematic structure of photosystem **3** with HOMO (bold) and LUMO (dashed) energy levels (from differential pulse voltammetry, normalized against -5.1 eV for Fc^+/Fc, see Fig. S3† and Table S1†; shaded circles and grey line indicate ascorbic acid and ITO as final acceptors, respectively), and with hole (h^+) and electron (e^-) transfer cascades for photoinduced charge separation and translocation in *p*- and *n*-transporting channels, respectively. (B) Molecular structure of photosystem **3**. (C) Schematic structure of control systems **1**, **2** and **4** (● = hydrazone from benzaldehyde, compare **6**). The structures shown are consistent with design, synthesis and results. However, they are idealized structures, defects will be repaired due to the dynamic covalent chemistry employed, but only to a certain extent.[24,42]

disulfide-exchange polymerization initiated by **5** (Fig. 2A). The fullerene stack exchangers **9**-**11** were equipped with an aldehyde and two ethyleneglycol chains to assure solubility in polar aprotic solvents for TSE (Figs. 1B, 2A, S1†).[27]

The preparation of components **5**-**11** required substantial multistep synthesis (Schemes S1-S3†). Detailed procedures and analytical data of all new compounds are provided in the Supporting Information. The HOMO and LUMO energies of the new TA and TE tetramers **6** and **8** were determined by differential pulse voltammetry and optical bandgaps, and found to be compatible with the construction of antiparallel three-component gradients (Figs. 1A, S2†, S3†, Table S1†).

The synthesis of the [3+3] photosystem **3** was launched with the deposition of initiator **5** on ITO (Fig. 2A, Schemes S4-S5†). The monolayer was characterized as described for previous systems (Fig. S4†), and the thiols were deprotected on the surface with DTT. For SOSIP, the activated monolayer **12** was incubated in solutions of TA propagator **6** under carefully optimized conditions (Figs. 2A, 2B, S5†, Table S2†). At sufficient thickness (judged from the absorption spectra, Fig. 2B), the obtained [1+0] photosystem **13** was incubated with TT propagator **7** to give [2+0] photosystem **14**, which in turn was incubated with TE propagator **8** to SOSIP the third component of the oriented gradient in [3+0] photosystem **15** (Figs. 2A, 2B, S6†). In all experiments, the oligothiophene absorption maximum at 435 nm of the final [3+0] photosystems **15** was set at $A \sim 0.3$-0.5 (Fig. 2B). For an ideal π-stack with 3.4 Å repeats, this calculated to thickness of 100-160 nm (ε_{max} ~4.3 x 10^4 M^{-1} cm^{-1}, Table S1†).

For TSE, the benzaldehyde templates in **15** were removed with excess hydroxylamine, and the large pores in **16** with reactive hydrazides along their walls were filled by reversible hydrazone formation with SB fullerene **9** (Figs. 2A, 2D, S7†). Part of the fullerene stack in [3+1] double-channel photosystem **17** was removed by controlled incubation with hydroxylamine, and the pores in photosystem were filled with DB fullerene **10** (Figs. 2A, 2C, 2D, S8†). Removal of part of the fullerenes in [3+2] photosystem **19** with hydroxylamine followed by incubation with DM fullerene **11** to fill the shallow pores in **20** gave the [3+3] photo- system **3** (Figs. 2D, S9†). The yield of each TSE reaction was determined from changes in the absorption spectra of the transparent electrodes, conditions were systematically optimized until >50% was reached (Figs. 2C, 2D, S7-S11†, Table S3†). The control photosystems **1**, **2** and **4** were prepared correspondingly.

Photocurrent generation was measured under routine conditions with the photosystems as working electrodes, a platinum wire as a counter electrode and ascorbic acid as a mobile hole transporter in solution (mobile hole transporters other than ascorbic acid were tested as well, triethanolamine gave clearly higher initial photocurrents but seemed to damage the surface of photosystem **3**). Results obtained under these conditions are not comparable with those from optimized optoelectronic devices but they are fully appropriate to evaluate and compare different multicomponent architectures.

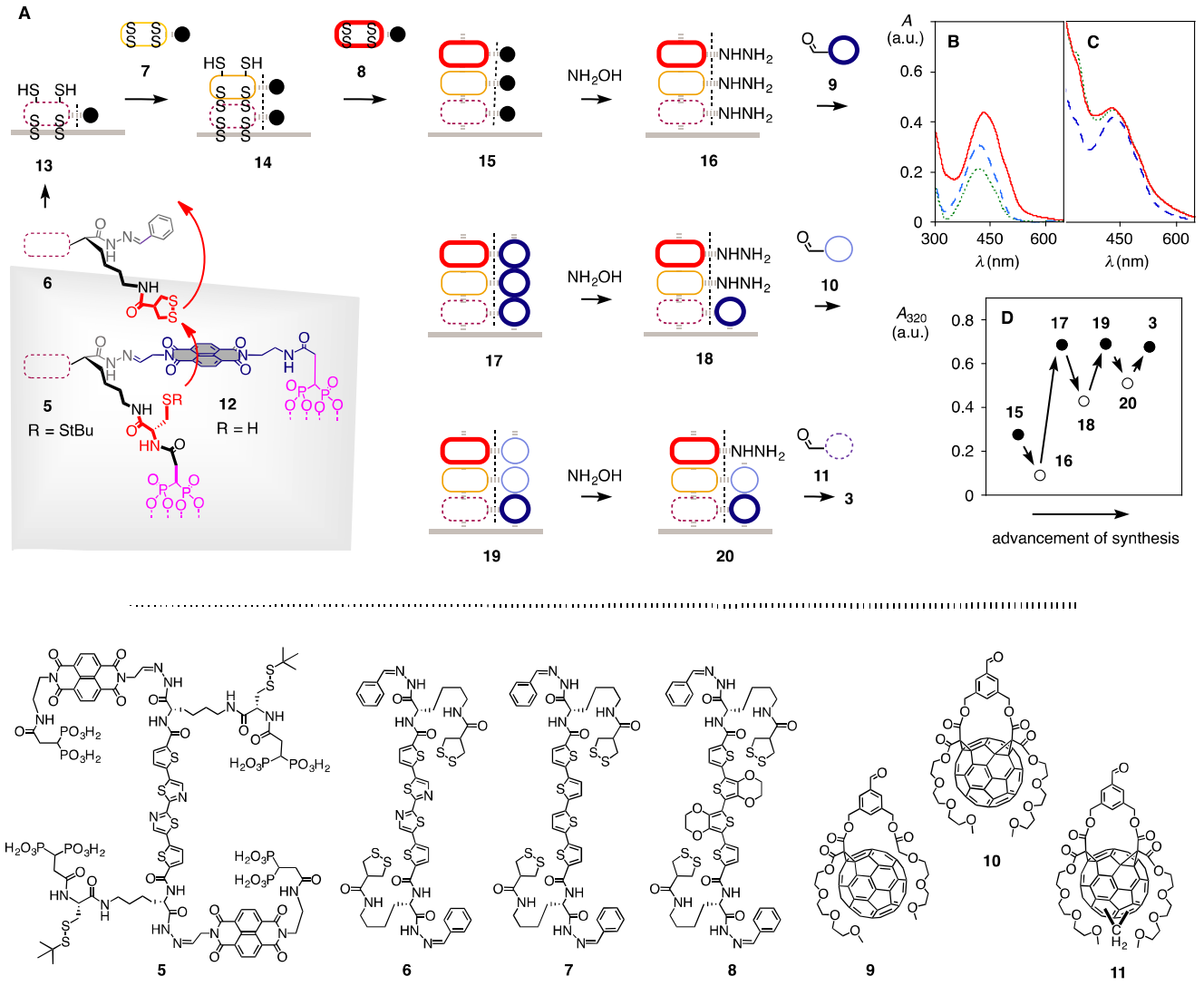

Fig. 2. Synthesis of antiparallel three-component gradients. (A) Synthetic scheme for [3+3] architecture **3** (see Figs. 1 and S5-S9† for full structures). (B) Absorption spectra of [1+0] architecture **13** (dotted), [2+0] **14** (dashed) and [3+0] **15** (solid). (C) Absorption spectra of [3+1] architecture **17** (dotted, green), intermediate **18** (dashed) and [3+2] **19** (solid, red). (D) Changes in absorption at 320 nm during TSE (compare Fig. 1 for structures).

Triple-gradient photosystem **3** generated clearly more short-circuit photocurrent density J_{SC} than double-gradient photosystem **2** (Fig. 3A, ● vs △, Table 1). The [2+2] photosystem **2** was in turn more active than the gradient-free [1+1] photosystem **1** (Fig. 3A, △ vs ○), which in turn was much more active than the single-channel [1+0] control **4** (Fig. 3A, ○ vs ◆). These gradual improvements demonstrated that each level of sophistication contributes to the activity of [3+3] photosystem **3**. The final triple-gradient double-channel photosystem **3** generated about 50-times more J_{SC} than the simplest [1+0] control **4**.

The quite remarkable increase of photoactivity by increasing number of components in the oriented antiparallel gradients could in part be rationalized by decreasing charge recombination efficiency η_{BR} (Fig. 3B, Table 1). Namely, the dependence of J_{SC} to the irradiation intensity I[32] revealed nearly perfect η_{BR} = 2% for [3+3] photosystem **3** (Fig. 3B, ●), slightly higher η_{BR} = 19% for [2+2] photosystem **2** (Fig. 3B, △) and even higher η_{BR} = 29% for [1+1] photosystem **1** (Fig. 3B, ○). More pronounced reduction of charge recombination by converting [2+2] to [3+3] photosystems, in comparison to [1+1] to [2+2] photosystems, supported the significance of the third component in the gradient.

Increasing charge mobility by increasing complexity was further implied by the temperature dependence of photocurrent J_{SC} (Fig. 3C).[33-35] According to Arrhenius plots, the activation energy E_a needed for photocurrent generation decreased with increasing sophistication of the charge-transfer cascades down to E_a = 121 meV of [3+3] photosystem **3** (Table 1). Here again, the addition of the third components significantly affected E_a.

Dark current measurements were of interest to explore the characteristics of antiparallel charge-transfer cascades for the function of the diode. The voltage needed to force charges to flow against the direction of the redox gradients is referred to as the turn-on voltage V_d. The turn-on voltage of the dark current increased with increasing sophistication of the charge-transfer

Table 1. Characteristics of double-channel photosystems with or without antiparallel gradients containing [n+m] components.

PS [a]		J_{SC} (μA cm^{-2}) [b]	η_{BR} (%) [c]	E_a (meV) [d]	n [e]	V_d (mV) [f]
1	[1+1]	2	29	209	2.58	-130
2	[2+2]	6	19	172	1.71	-190
3	[3+3]	12	2	121	1.48	-290

[a] Double-channel photosystems with [3+3] = triple gradient, [2+2] = double gradient and [1+1] = without gradient, see Fig. 1 for structures. [b] Short-circuit photocurrent density J_{SC} generated by irradiation with white light (Fig. 3A), [c] bimolecular charge recombination efficiencies η_{BR} from the dependence of J_{SC} on irradiation intensity (Fig. 3B), [d] activation energy E_a from the dependence of J_{SC} on temperature (Fig. 3C), and [e] ideality factor n and [f] turn-on voltage V_d from the voltage dependence of the dark current (Fig. 3D).

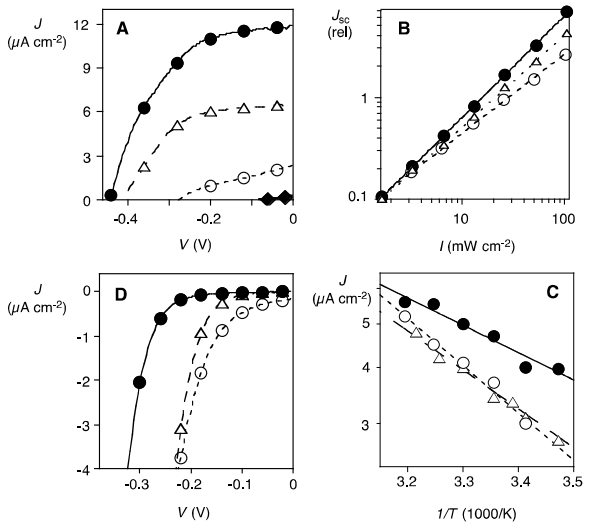

Fig. 3. Evaluation of antiparallel three-component gradients. (A) Dependence of photocurrent density J on voltage V (solar simulator, W = 100 mW, 50 mM ascorbic acid, 100 mM Na_2SO_4, Pt counter electrode) for **3** (●), **2** (△), **1** (○) and **4** (◆). (B) Dependence of short-circuit photocurrent density J_{SC} on the irradiation intensity I for **3** (●), **2** (△) and **1** (○) (normalized to J_{SC} = 0.1 μA cm^2 at I = 1.63 mW cm^2 to facilitate comparison). (C) Arrhenius plot of J_{SC} on temperature T for **3** (●), **2** (△) and **1** (○). (D) Dependence of the dark current density J on voltage V for **3** (●), **2** (△) and **1** (○).

cascade from V_d = -130 mV for gradient-free double-channel [1+1] photosystem **1** to V_d = -290 mV for triple-gradient [3+3] photosystem **3** (Fig. 3D, Table 1). This result confirmed that uphill charge flow becomes harder with more components in the gradient, and that the presence of the third component of the gradient is of decisive importance. The significant dependence of turn-on voltage V_d on the sophistication of the antiparallel gradients naturally influences also the open circuit voltage V_{OC} of the photocurrents very positively (Fig. 3A).

From the exponential increase of the dark current density J around the turn-on voltage, formal ideality factors n were determined.[36,37] Decreasing ideality factors with increasing number of components in the redox gradient confirmed that the lessons learned from η_{BR} and E_a for photocurrents apply also for dark currents (Fig. 3D, Table 1). Namely, each component added to antiparallel charge-transfer cascades helps to minimize charge trapping and recombination.

Note that most analytical methods used here to quantify the results have been developed in the context of different configurations. Although consistent and comparable within the reported series, the obtained values should not be compared with those obtained with different configurations, and their meaning should be considered with appropriate caution.

Taken together, functional analysis reveals that each level of sophistication engineered into multicomponent architectures improves all aspects of their activity consistently and significantly. Photocurrents increase steadily from the addition of a second co-axial channel over the introduction of redox gradients composed of two components to the final three-component charge-transfer cascades in both channels. As in the natural photosystems, charge recombination decreases toward perfection with increasing sophistication of the antiparallel gradients, driving holes and electrons apart right after their generation with light. Thermal activation energies and ideality factors decrease correspondingly, whereas the turn-on voltages to move the charges uphill increase with increasing sophistication of the gradients.

Finally, we would like to highlight the synthetic aspect of this work. Compared to high standards with small molecules, the synthetic organic chemistry of large systems is poorly developed. To help improving on this situation, we have introduced SOSIP,[23] TSS[24] and TSE[25] as general synthetic methods. The important achievement[1] reported herein demonstrates that these new methods provide synthetic access to the transcription of one of the most complex lesson from nature to organic materials, i.e., oriented antiparallel three-component gradients. The key to success was the directional use of orthogonal dynamic covalent bonds,[38-41] *i.e.,* disulfide exchange for SOSIP[23] and hydrazone exchange for TSE,[25] in combination with molecular recognition, self-sorting[24] and self-repair.[42] The development of analytical methods to characterize multicomponent architectures at this level of complexity beyond functional feedback loops emerges as a challenge for the future. The results from functional analysis demonstrate that these synthetic efforts to learn how to construct functional systems of highest sophistication are worthwhile and are thus expected to stimulate progress in the field in the broadest sense.

Acknowledgements

We thank the NMR and the Sciences Mass Spectrometry (SMS) platforms for services, and the University of Geneva, the European Research Council (ERC Advanced Investigator), the National Centre of Competence in Research (NCCR) Chemical Biology, the NCCR Molecular Systems Engineering and the Swiss NSF for financial support.

References

1 R. Bhosale, N. Sakai, J. Mísek and S. Matile, *Chem. Soc. Rev.*, 2010, **39**, 138-149, and references therein.
2 F. Würthner, *Science*, 2006, **314**, 1693-1694.
3 D. M. Bassani, L. Jonusauskaite, A. Lavie-Cambot, N. D. McClenaghan, J.-L. Pozzo, D. Ray and G. Vives, *Coord. Chem. Rev.*, 2010, **254**, 2429-2445.
4 T. Marangoni and D. Bonifazi, *Nanoscale*, 2013, **5**, 8837-8851.
5 D. M. Guldi, I. Zilbermann, G. Anderson, A. Li, D. Balbinot, N. Jux, M. Hatzimarinaki, A. Hirsch and M. Prato, *Chem. Commun.*, 2004, **39**, 726-727.

6 M. Morisue, S. Yamatsu, N, Haruta and Y. Kobuke, *Chem.-Eur. J.*, 2005, **11**, 5563-5574.
7 S. O. Krabbenborg and J. Huskens, *Angew. Chem. Int. Ed.*, 2014, **53**, 9152-9167.
8 P. Parkinson, C. E. Knappke, N. Kamonsutthipaijit, K. Sirithip, J. D. Matichak, H. L. Anderson and L. M. Herz, *J. Am. Chem. Soc.*, 2014, **136**, 8217-8220.
9 H. Hayashi, I. V. Lightcap, M. Tsujimoto, M. Takano, T. Umeyama, P. V. Kamat and H. Imahori, *J. Am. Chem. Soc.*, 2011, **133**, 7684-7687.
10 F. Garo and R. Häner, *Angew. Chem. Int. Ed.*, 2012, **51**, 916-619.
11 P. M. Beaujuge and J. M. J. Fréchet, *J. Am. Chem. Soc.*, 2011, **133**, 20009-20029.
12 T. Aida, E. W. Meijer and S. I. Stupp, *Science,* 2012, **335**, 813-817.
13 M. R. Wasielewski, *Acc. Chem. Res.*, 2009, **42**, 1910-1921.
14 A. Mishra and P. Bäuerle, *Angew. Chem. Int. Ed.*, 2012, **51**, 2020-2067.
15 R. Kumar, J. MacDonald, T. Singh, L. Waddington and A. Holmes, *J. Am. Chem. Soc.*, 2011, **133**, 8564-8573.
16 M. Urbani, J. Iehl, I. Osinska, R. Louis, M. Holler and J.-F. Nierengarten, *Eur. J. Org. Chem.*, 2009, 3715-3725.
17 Y. Zhang, Y. Matsuo, C.-Z. Li, H. Tanaka and E. Nakamura, *J. Am. Chem. Soc.*, 2011, **133**, 8086-8089.
18 D. Bonifazi, O. Enger and F. Diederich, *Chem. Soc. Rev.*, 2007, **36**, 390-414.
19 F. D'Souza and O. Ito, *Chem. Commun*., 2009, **45**, 4913-4928.
20 S. S. Babu, H. Möhwald and T. Nakanishi, *Chem. Soc. Rev*., 2010, **39**, 4021-4035.
21 F. Giacalone and N. Martín, *Adv. Mater*., 2010, **22**, 4220-4248.
22 N. Sakai, R. Bhosale, D. Emery, J. Mareda and S. Matile, *J. Am. Chem. Soc.*, 2010, **132**, 6923-6925.
23 N. Sakai, M. Lista, O. Kel, S.-I. Sakurai, D. Emery, J. Mareda, E. Vauthey and S. Matile, *J. Am. Chem. Soc.*, 2011, **133**, 15224-15227.
24 E. Orentas, M. Lista, N.-T. Lin, N. Sakai and S. Matile, *Nat. Chem.*, 2012, **4**, 746-750.
25 N. Sakai and S. Matile, *J. Am. Chem. Soc.*, 2011, **133**, 18542-18545.
26 A. Bolag, H. Hayashi, P. Charbonnaz, N. Sakai and S. Matile, *ChemistryOpen*, 2013, **2**, 55-57.
27 A. Bolag, J. Lopez-Andarias, S. Lascano, S. Soleimanpour, C. Atienza, N. Sakai, N. Martín and S. Matile, *Angew. Chem. Int. Ed.*, 2014, **53**, 4890-4895.
28 M. Turbiez, P. Frère, M. Allain, C. Videlot, J. Ackermann and J. Roncali, *Chem.-Eur. J.*, 2005, **11**, 3742-3752.
29 P. M. Beaujuge, C. M. Amb and J. R. Reynolds, *Acc. Chem. Res.*, 2010, **43**, 1396-1407.
30 X. Guo, J. Quinn, Z. Chen, H. Usta, Y. Zheng, Y. Xia, J. W. Hennek, R. P. Ortiz, T. J. Marks and A. Facchetti, *J. Am. Chem. Soc.*, 2013, **5**, 1986-1996.
31 W. Li, H. E. Katz, A. J. Lovinger and J. G. Laquindanum, *Chem. Mater.*, 1999, **11**, 458-465.
32 L. J. A. Koster, M. Kemerink, M. M. Wienk, K. Maturová and R. A. J. Janssen, *Adv. Mater.*, 2011, **23**, 1670-1674.
33 B. J. Kim, H. Yu, J. K. Oh, M. S. Kang and J. H. Cho, *J. Phys. Chem. C,* 2013, **117**, 10743-10749.
34 V. Coropceanu, J. Cornil, D. A. da Silva Filho, Y. Olivier, R. Silbey and J.-L. Bredas, *Chem. Rev.*, 2007, **107**, 926-952.
35 N. Sakai, P. Charbonnaz, S. Ward and S. Matile, *J. Am. Chem. Soc.*, 2014, **136**, 5575-5578.
36 G. A. H. Wetzelaer, M. Kuik, M. Lenes and P. W. M. Blom, *Appl. Phys. Lett.*, 2011, **99**, 153506.
37 J. H. Lee, S. Cho, A. Roy, H.-T. Jung and A. J. Heeger, *Appl. Phys. Lett.*, 2010, **96**, 163303.
38 A. Wilson, G. Gasparini and S. Matile, *Chem. Soc. Rev.*, 2014, **43**, 1948-1962.
39 J.-M. Lehn, *Top. Curr. Chem*., 2012, **322**, 1-32.
40 J. Li, P. Nowak and S. Otto, *J. Am. Chem. Soc.*, 2013, **135**, 9222-9239.
41 S. P. Black, J. K. M. Sanders and A. R. Stefankiewicz, *Chem. Soc. Rev.*, 2014, **43**, 1861-1872.
42 M. Lista, J. Areephong, N. Sakai and S. Matile, *J. Am. Chem. Soc.*, 2011, **133**, 15228-15231.

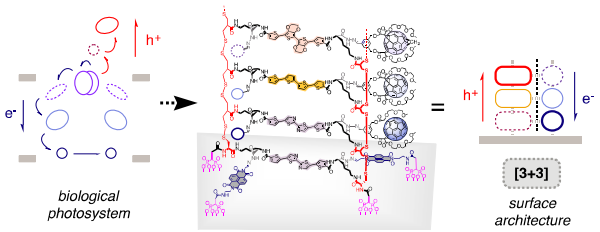

Synthetic methods are reported to transcribe complex characteristics of biological systems into organic materials on an unprecedented level of sophistication.